Applicability of deep learning-based reconstruction trained by brain and knee 3T MRI to lumbar 1.5T MRI

Nobuo Kashiwagi[1] ⓘ, Hisashi Tanaka[2], Yuichi Yamashita[3], Hiroto Takahashi[4], Yoshimori Kassai[5] ⓘ, Masahiro Fujiwara[6] and Noriyuki Tomiyama[6]

Abstract

Background: Several deep learning-based methods have been proposed for addressing the long scanning time of magnetic resonance imaging. Most are trained using brain 3T magnetic resonance images, but is unclear whether performance is affected when applying these methods to different anatomical sites and at different field strengths.
Purpose: To validate the denoising performance of deep learning-based reconstruction method trained by brain and knee 3T magnetic resonance images when applied to lumbar 1.5T magnetic resonance images.
Material and Methods: Using a 1.5T scanner, we obtained lumber T2-weighted sequences in 10 volunteers using three different scanning times: 228 s (standard), 119 s (double-fast), and 68 s (triple-fast). We compared the images obtained by the standard sequence with those obtained by the deep learning-based reconstruction-applied faster sequences.
Results: Signal-to-noise ratio values were significantly higher for deep learning-based reconstruction-double-fast than for standard and did not differ significantly between deep learning-based reconstruction-triple-fast and standard. Contrast-to-noise ratio values also did not differ significantly between deep learning-based reconstruction-triple-fast and standard. Qualitative scores for perceived signal-to-noise ratio and overall image quality were significantly higher for deep learning-based reconstruction-double fast and deep learning-based reconstruction-triple-fast than for standard. Average scores for sharpness, contrast, and structure visibility were equal to or higher for deep learning-based reconstruction-double-fast and deep learning-based reconstruction-triple-fast than for standard, but the differences were not statistically significant. The average scores for artifact were lower for deep learning-based reconstruction-double-fast and deep learning-based reconstruction-triple-fast than for standard, but the differences were not statistically significant.
Conclusion: The deep learning-based reconstruction method trained by 3T brain and knee images may reduce the scanning time of 1.5T lumbar magnetic resonance images by one-third without sacrificing image quality.

[1]Department of Future Diagnostic Radiology, Osaka University Graduate School of Medicine, Osaka, Japan
[2]Division of Health Science, Department of Medical Physics and Engineering, Osaka University Graduate School of Medicine, Osaka, Japan
[3]Canon Medical Systems Corporation, Kanagawa, Japan
[4]Center for Twin Research, Osaka University Graduate School of Medicine, Osaka, Japan
[5]Canon Medical Systems Corporation, Tochigi, Japan
[6]Department of Radiology, Osaka University Graduate School of Medicine, Osaka, Japan

Corresponding author:
Nobuo Kashiwagi, Department of Future Diagnostic Radiology, Osaka University Graduate School of Medicine, Osaka, Japan.
Email: n-kashiwagi@radiol.med.osaka-u.ac.jp

Introduction

Magnetic resonance imaging (MRI) is an effective imaging modality for identifying various disorders through the body because of the variety of contrast mechanisms and because it requires no ionizing radiation. However, a major disadvantage of MRI is the long acquisition time, which is required for optimal image quality. One of the main approaches to address this shortcoming of MRI is post-processing denoising,

which recovers the degradation in image quality associated with the reduced acquisition time. Recent advances in deep learning have improved the computational cost, training time, and amount of data required, and have led to its application to medical imaging denoising,[1,2] as reported in several publications that have achieved robust denoising performances in magnetic resonance (MR) images.[3–13] However, most have been trained using brain images acquired on a 3T machine and applied to brain images also on a 3T machine.[3–13] However, clinically, the contrast of MR images can vary because of differences in the scan protocol, field strength, and anatomical location, and it is unclear whether this variability affects the performance of these denoising methods.[14] To ensure robustness against these variations, deep learning-based reconstruction (DLR) methods have been proposed to perform denoising only for high-frequency components that contain detailed information about structures and most of the noise, while leaving low-frequency components containing the image contrast information.[15]

The proposed DLR method (Advanced intelligent Clear-IQ Engine, Canon Medical Systems Corporation, Tochigi, Japan) has been trained using brain and knee 3T MR images and has been confirmed as being able to achieve significant noise reduction for brain 3T MR images while preserving the image quality.[15,16] However, the applicability of the proposed DLR method to MR images of other anatomical sites and at different field strengths has not been investigated. The purpose of this study was to evaluate the applicability of the proposed DLR method when applied to lumbar 1.5T MRI.

Material and Methods

Subjects

The study protocol was approved by the Institutional Review Board and informed consent was obtained from participants before they entered the study. Ten healthy male volunteers, with a mean age of 41 years (range 24–57 years), participated in this study.

MRI data acquisition

We performed lumbar spine studies using a 1.5T MRI system (Vantage Orian 1.5T, Canon Medical Systems Corporation) with a 32-element phased-array surface spine coil. First, we performed standard turbo spin-echo T2-weighted sequences with an acquisition time of 228 s, as used for routine clinical examination. Second, by reducing the number of excitations (NEX) and the combined application of reduced NEX and

Table 1. Imaging parameters.

	Standard	Double-fast	Triple-fast
TR/TE (ms)	3400/84		
Echo train length	17		
Echo space (ms)	10.5		
Bandwidth (HZ)	245.1		
Slice thickness (mm)	3		
FOV phase (mm)	300		
FOV read (mm)	270		
Matrix (phase × read)	320 × 384		
NEX	2	1	1
CS factor	None	None	1.8
Scan time (s)	228	119	68

NEX: number of excitations; CS: compressed sensing, TR: repetition time, TE: echo time, FOV: field of view.

compressed sensing, we performed two accelerated sequences with scanning times of 119 s (shortened by about one-half) and 68 s (shortened by about one-third). For the compressed sensing, using a commercialized application (compressed SPEEDER, Canon Medical Systems Corporation), we randomly reduced sampling data to 55% (reduction factor of 1.8) by interactive compressed sensing optimization with least absolute and selection operator regression. The other parameters were identical, and the details of the sequencing parameters are described in Table 1. Subsequently, we applied the DLR to the two accelerated sequences and obtained the following five sets of images: images obtained by standard sequences (standard), images obtained with the accelerated sequence shortened by about one-half (double-fast), DLR-applied images obtained with the accelerated sequence shortened by about one-half (DLR-double-fast), images obtained with the accelerated sequence shortened by about one-third (triple-fast), and DLR-applied images obtained by accelerated sequence shortened by about one-third (DLR-triple-fast).

DLR method

The noise reduction in this study was performed using a commercial DLR tool (Advanced Intelligent Clear-IQ Engine, Canon Medical Systems), the details of which have been reported.[15] The DLR has three layers, and the architecture is shown in Fig. 1. The DLR derives 49 components with a fixed 7×7 discrete cosine transform (DCT) basis. After the separation of the zero-frequency component of the DCT and the other 48 high-frequency components, soft shrinkage was applied to the later components. In the feature conversion layer, 3×3 convolution and soft shrinkage were applied 22 times to the 48 high-frequency components, and the zero-frequency component of the DCT
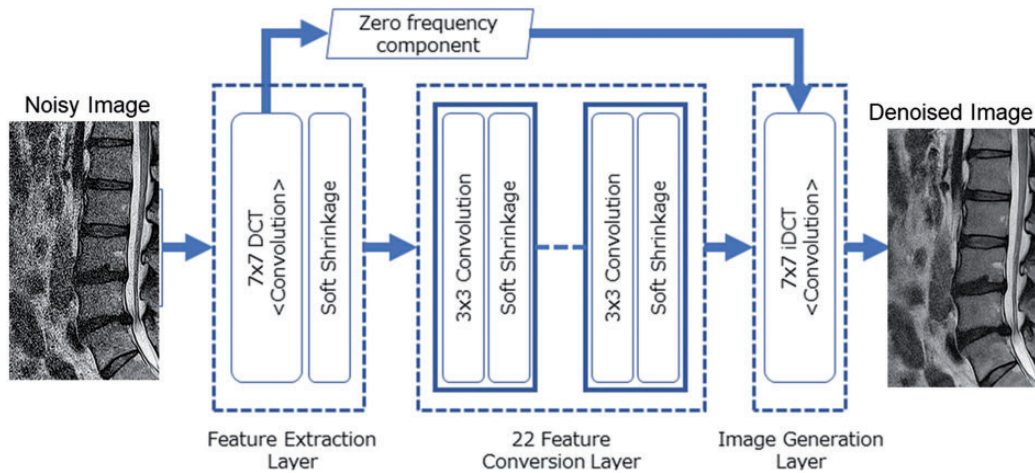
Fig. 1. Deep learning-based reconstruction (DLR) architecture. Among the 49 components derived in the feature extraction layer, the 48 high-frequency components undergo soft shrinkage and repeated 3×3 convolutions and soft shrinkages. By contrast, the zero-frequency component takes a collateral pathway. In the image generation layer, the denoised high-pass components and bypassed zero-frequency component are combined.
DCT: discrete cosine transform.

went through a separate collateral pathway. In the final image-generation layer, the high-pass component and the bypassed zero-frequency component were combined to generate denoised images by deconvolution using a 7×7 DCT kernel. The main idea underlying this DLR method is the selective processing of the high-frequency component, which is expected to allow noise removal while preserving the image contrast and detailed structure.

Quantitative image analysis

Analysis of the regions of interest (ROIs) was performed by a board-certified neuroradiologist (NK) with 25 years of experience. In the central slice of the spine, oval-shaped ROIs of 30 mm^2 were placed on the background air, retroperitoneal fat at the first sacral vertebral level, cerebrospinal fluid (CSF) at the first sacral vertebral level, second lumbar vertebra, L1–2 intervertebral disc, and cord at the 12th thoracic vertebral level. ROIs were also placed on the paravertebral muscle in the paramedian slice depicting the right intervertebral foramina (Fig. 2). For each tissue, we calculated the signal-to-noise ratio (SNR) and contrast-to-noise ratio of the muscle (CNR) using the following formulas from the literature:[17,18] $SNR = SI_{tissue}/SD_{background\,air}$, $CNR = SI_{tissue} - SI_{muscle}/SI_{muscle}$. SI was taken as the average signal intensity of the ROIs, and SD as the standard deviation of the ROIs.

Qualitative image analysis

Three independent neuroradiologists (MF, HT, and HT who had 6, 17, and 26 years of experience in

neuroradiology, respectively) evaluated the five sets of images. After the MR images were presented in random order, they were evaluated independently without knowledge of the sequence parameter. The readers assessed the perceived SNR, sharpness, contrast, structure visibility, artifact, and overall image quality relative to the control images obtained by the standard sequence using a five-point scale (1 = obviously inferior; 2 = slightly inferior; 3 = equivalent; 4 = slightly superior; 5 = obviously superior).

Statistical analysis and comparison between the groups

All statistical calculations were performed using IBM SPSS Statistics for Windows (version 24). For quantitative analysis, all numerical values are reported as the average ± SD. For qualitative analysis, median values of the scores from the three independent neuroradiologists were assessed. First, we compared DLR-applied accelerated images to their DLR-nonapplied counterparts (double-fast versus DLR-double-fast, triple-fast versus DLR-triple-fast) to confirm the denoising performance of the DLR. Second, we compared DLR-applied accelerated images to standard images (standard versus DLR-double-fast, standard versus DLR-triple-fast) to validate the feasibility of the DLR method for shortening the scanning time.

Intergroup differences were examined using the two-sided Wilcoxon signed-rank test followed by the Benjamini–Hochberg procedure to control the false discovery rate in multiple comparisons. Differences with $q < 0.05$ were considered to be significant.[19]
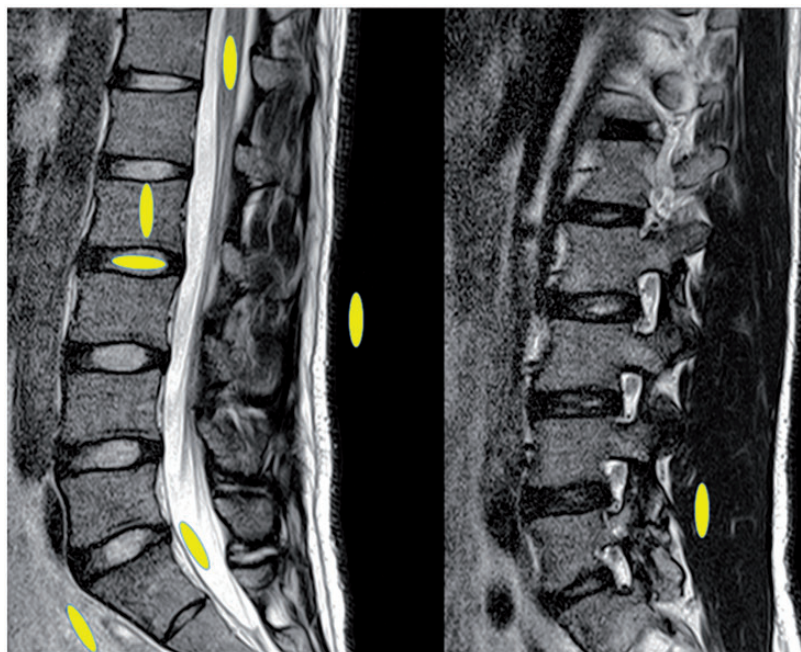
Fig. 2. Measurements of regions of interest (ROIs) in a volunteer. ROIs were placed on the retroperitoneal fat, CSF, vertebra, disc, cord, background air, and paravertebral muscle.

Results

Quantitative analysis

The results of the quantitative assessments are shown in Table 2 and Fig. 3. The average SNR values for all tissues were highest on DLR-double-fast, followed by DLR-triple-fast or standard, double-fast, and triple-fast. In the comparison between DLR-applied accelerated images and their DLR-nonapplied counterparts, the SNR values for all tissues were significantly higher for DLR-applied accelerated images than for their non-applied counterparts, indicating the effective denoising performance of the DLR. The comparison between DLR-applied accelerated images and standard images indicated that adequate restoration decreased the SNR caused by shortened scanning times. The SNR values for all tissues were significantly higher for DLR-double-fast than for standard. The SNR values for all tissues did not differ significantly between DLR-triple-fast and standard, but the average SNR values for the vertebra, disc, cord, and muscle were higher for DLR-triple-fast than for standard.

Analysis of the CNR indicated preservation of tissue contrast on DLR-applied accelerated images. The CNR values for all tissues were significantly higher for DLR-applied accelerated images than for their DLR-nonapplied counterparts. The CNR values for fat and CSF were significantly higher for DLR-double-fast than for standard. Those for vertebra, disc and cord were higher for DLR-double-fast than for standard on average, and the differences were not statistically significant. The CNR values for all tissues differed only slightly between DLR-triple-fast and standard.

Qualitative analysis

The qualitative scores are shown in Table 3 and Fig. 4, and representative images are shown in Figs 5 and 6. The average scores for perceived SNR, sharpness, contrast, structure visibility, and overall image quality were highest on DLR-double-fast or DLR-triple-fast, followed by standard, double-fast, and triple-fast. The average scores for artifact were highest on standard and double-fast, followed by triple-fast, DLR-double-fast, and DLR-triple-fast.

In the comparison between DLR-applied accelerated images and their DLR-nonapplied counterparts, the scores for perceived SNR, sharpness, contrast, and overall image quality were significantly higher for DLR-applied accelerated images than for their DLR-nonapplied counterparts. The scores for structure visibility were significantly higher for DLR-triple-fast than for triple-fast. The scores for artifacts did not significantly differ between these groups.

In the comparison between DLR-applied accelerated images and standard images, the scores for perceived SNR and overall image quality were significantly higher for DLR-double-fast and DLR-triple-fast than for standard. The scores for sharpness,

Table 2. Quantitative values for SNR and CNR.

	SNR value				
	(1) Standard	(2) Double-fast	(3) DLR-double-fast	(4) Triple-fast	(5) DLR-triple-fast
Fat	111.3 ± 44.0	73.1 ± 29.2	123.0 ± 47.8	64.4 ± 17.2	109.9 ± 25.6
CSF	140.8 ± 51.0	92.7 ± 36.8	155.8 ± 60.0	81.6 ± 18.1	140.2 ± 26.0
Vertebra	59.7 ± 20.3	39.7 ± 14.3	66.2 ± 23.0	35.8 ± 9.6	60.5 ± 14.4
Disc	46.0 ± 14.1	30.5 ± 8.7	50.5 ± 13.8	27.9 ± 8.1	46.8 ± 14.6
Cord	48.9 ± 18.2	32.6 ± 12.1	54.4 ± 19.7	28.9 ± 7.5	49.4 ± 12.1
Muscle	16.6 ± 9.8	11.1 ± 7.0	18.5 ± 11.4	10.3 ± 4.1	21.6 ± 14.0
	q Values				
	(2) vs (3)	(4) vs (5)	(1) vs (3)	(1) vs (5)	
Fat	**<0.01**	**<0.01**	**<0.01**	0.60	
CSF	**<0.01**	**<0.01**	**<0.01**	0.32	
Vertebra	**<0.01**	**<0.01**	**0.02**	0.49	
Disc	**<0.01**	**<0.01**	**<0.01**	0.70	
Cord	**<0.01**	**<0.01**	**0.04**	0.10	
Muscle	**<0.01**	**<0.01**	**0.02**	0.09	
	CNR value				
	(1) Standard	(2) Double-fast	(3) DLR-double-fast	(4) Triple-fast	(5) DLR-triple-fast
Fat	94.7 ± 35,6	62.0 ± 23.3	104.5 ± 38.3	54.0 ± 14.7	88.3 ± 26.1
CSF	124.2 ± 41.5	81.6 ± 30.1	137.4 ± 49.0	71.3 ± 14.6	118.6 ± 23.5
Vertebra	43.0 ± 13.6	28.5 ± 9.3	47.8 ± 14.8	25.5 ± 9.3	38.9 ± 15.7
Disc	29.30 ± 12.5	14.9 ± 8.2	32.0 ± 14.9	17.6 ± 8.5	25.2 ± 17.8
Cord	32.3 ± 9.9	21.5 ± 6.5	36.0 ± 11.0	18.6 ± 5.8	24.9 ± 12.5
	q Values				
	(2) vs (3)	(4) vs (5)	(1) vs (3)	(1) vs (5)	
Fat	**<0.01**	**<0.01**	**0.03**	0.85	
CSF	**<0.01**	**<0.01**	**<0.01**	1.00	
Vertebra	**<0.01**	**0.01**	0.05	0.92	
Disc	**<0.01**	**0.04**	0.09	0.72	
Cord	**<0.01**	**<0.01**	0.43	0.72	

CSF: cerebrospinal fluid; DLR: deep learning-based reconstruction; CNR: contrast-to-noise ratio.
Note: Data are presented as average ± standard deviation of 10 volunteers.
Statistically significant values are shown in bold.

contrast, structure visibility, and artifacts did not differ significantly between these groups.

Discussion

In an effort to counter the image degradation cause by reducing the NEX, we applied the DLR to 1.5T lumbar T2-weighted images and found that its application allowed the scanning time to be shortened by one-half. The observed performance of the DLR in the current study was almost equal to that when applied to 3T brain MR images in a preceding study. In that study, the DLR allowed the scanning time of 3T brain MR images to be shortened by 60%.[15] In addition, the combination of the DLR with compressed sensing allowed us to shorten the scanning time by one-third without sacrificing image quality. These results suggest two clinical impacts. First, the time saving provided by the DLR increases the clinical utility of spinal MR imaging and alleviates the burden on the patient by shortening the scan time. This is particularly important in patients who are intolerant to the examination position or emergent condition. Second, the applicability of the DLR to different anatomical site or a different field strength from that used for the original training suggests that this method can be generalized to other applications.

When applying the DLR trained using brain and knee MR images at 3T field strength to lumbar MR
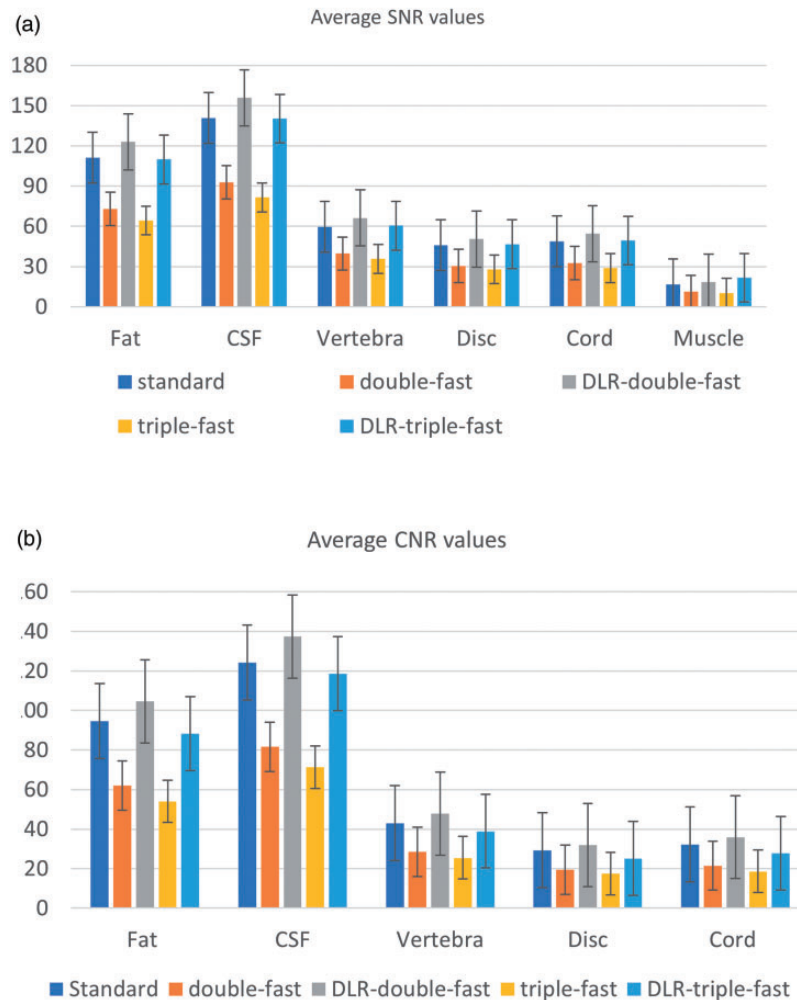
Fig. 3. Quantitative scores for five sets of images. (a) Average SNR values. The average SNR values for all tissues are lower for double-fast and triple-fast than for standard. After the DLR application, those for all tissues become higher for DLR-double-fast than for standard. Those for the vertebra, disc, cord, and muscle are slightly higher for DLR-triple-fast than for standard. (b) Average CNR values. The average CNR values for all tissues are lower for double-fast and triple-fast than for standard. After the DLR application, those become higher for DLR-double-fast than for standard and are slightly lower for DLR-triple-fast than for standard.
CSF: cerebrospinal fluid; DLR: deep learning-based reconstruction; CNR: contrast-to-noise ratio.

images at 1.5T, the following different conditions may affect the feasibility of the DLR. First is the inherent lower noise level in MR images acquired at 1.5T.[20,21] Second is the greater inhomogeneity of signal strength in spinal MR images because spinal MR images using the phased-array surface coil which has a lower coil sensitivity toward the deeper portions from the surface compared with brain MR images obtained using a phased-array head coil.[22,23] Third is the blurring effect, which reflects loss of information about spatial resolution and the common concern of denoising methods of MR images.[5,8,14] Uetani et al. reported that, in contrast to the usual denoising methods such as filtering or transform methods, deep learning-based denoising can overcome the adverse effect of denoising because it can learn anatomical structure.[16] However,

the concern remained in the current study because the DLR was applied to different anatomical sites from those used in the original training.

In the current study, we found that the DLR achieved significant elevation of the SNR without decreasing the tissue contrast. These results suggest that the specialized learning process, which involves selecting a high-frequency domain, worked in accordance with the intention to preserve the inherent tissue contrast, which exists mainly in the low-frequency domain.

The further reduction in the scanning time by the combination of the DLR and compressed sensing is consistent with the results of a recent report.[17] The image degradation accompanying compressed sensing is caused mainly by noise amplification, which increases logarithmically with the reduction factor of

Table 3. Qualitative scores for five sets of images.

	Qualitative scores				
	(1) Standard	(2) Double-fast	(3) DLR-double-fast	(4) Triple-fast	(5) DLR-triple-fast
Perceived SNR	3.1 ± 0.3	1.9 ± 0.3	4.0 ± 0	1.2 ± 0.4	4.0 ± 0
Sharpness	3.0 ± 0	2.2 ± 0.6	3.4 ± 0.5	1.0 ± 0	3.2 ± 0.4
Contrast	3.0 ± 0	2.4 ± 0.7	3.5 ± 0.5	1.4 ± 0.7	3.1 ± 0.6
Structure visibility	3.0 ± 0	2.8 ± 0.6	3.0 ± 0	2.5 ± 0.5	3.1 ± 0.3
Artifact	3.0 ± 0	3.0 ± 0	2.7 ± 0.5	2.8 ± 0.4	2.5 ± 0.5
Overall image quality	3.0 ± 0	2.2 ± 0.6	3.9 ± 0.3	1.0 ± 0	3.7 ± 0.5
	q Values				
	(2) vs (3)	(4) vs (5)	(1) vs (3)	(1) vs (5)	
Perceived SNR	**<0.01**	**<0.01**	**<0.01**	**<0.01**	
Sharpness	**<0.01**	**<0.01**	0.13	0.50	
Contrast	**0.02**	**0.02**	0.08	1.00	
Artifact	0.25	0.25	0.25	0.25	
Structure visibility	0.24	**<0.01**	1.00	0.24	
Overall image quality	**<0.01**	**<0.01**	**<0.01**	**0.02**	

SNR: signal-to-noise ratiol; DLR: deep learning-based reconstruction; CNR: contrast-to-noise ratio.
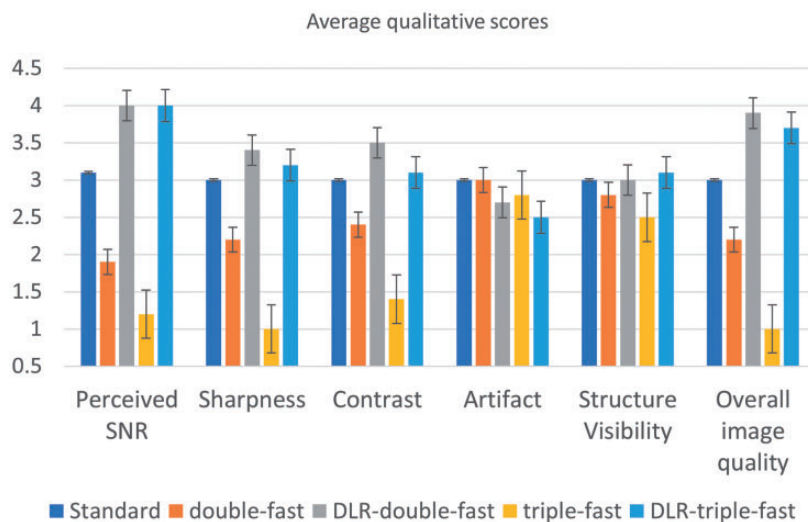Note: Data are presented as average ± standard deviation of 10 volunteers.

Fig. 4. Qualitative scores for five sets of images. Except for artifact, the average scores are lower for double-fast and triple-fast than for standard. After the DLR application, those for DLR-double-fast and DLR-triple-fast become equal to or higher than for standard. For artifact, the average scores for DLR-applied images are slightly lower than for DLR-nonapplied images.
SNR: signal-to-noise ratio; DLR: deep learning-based reconstruction.

compressed sensing.[24,25] Therefore, the noise amplification accompanying the compressed sensing was also controlled by the DLR and resulted in the synergic effect of reducing the scanning time.

Although the differences were nonsignificant, the average scores for artifact were lower for DLR-applied images than for DLR-nonapplied images. The artifact related to undersampling of the k-space in compressed sensing could not be removed by the DLR and was accentuated after the removal of noise (Fig. 5(b)).

This may be explained by the lack of an image domain from the under-sampled k-space data in the training data used for the DLR in our study.[15] To address this issue, further learning trained using under-sampled data may be warranted.[7–10] In the current study, motion artifact played no role because the study participants were healthy. Therefore, the potential resistance of DLR-applied accelerated sequence to motion artifact may result in less artifact overall in the clinical situations.
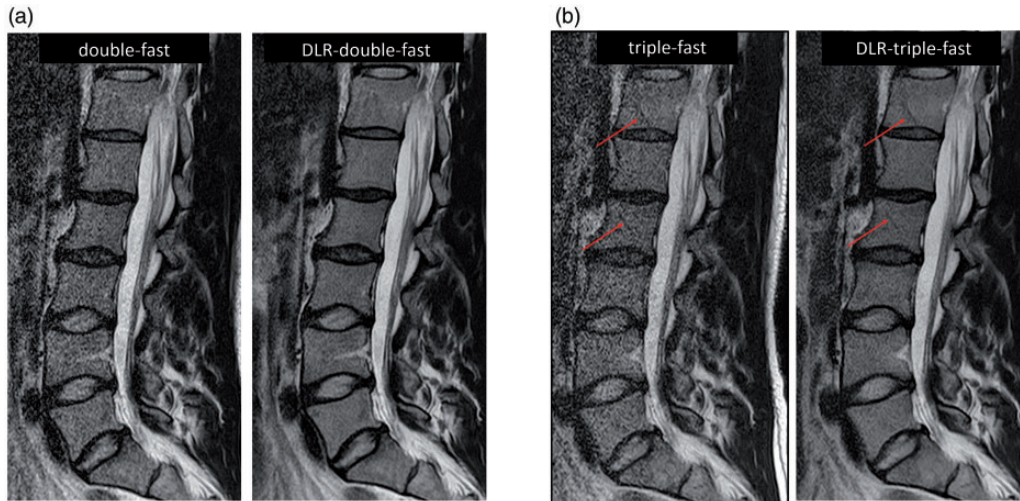
Fig. 5. Visual comparison between DLR-nonapplied accelerated images and DLR-applied accelerated images. (a) Visual comparison between double-fast and DLR-double-fast. Compared with the noisy accelerated image using reduced NEX (double-fast), the image quality is improved for the DLR-applied accelerated image (DLR-double-fast). (b) Visual comparison between triple-fast and DLR-triple-fast. DLR application (DLR-triple-fast) recovers the degenerated image quality associated with reduced NEX and compressed sensing. However, streaky artifacts caused by compressed sensing are maintained (arrows).
DLR: deep learning-based reconstruction.
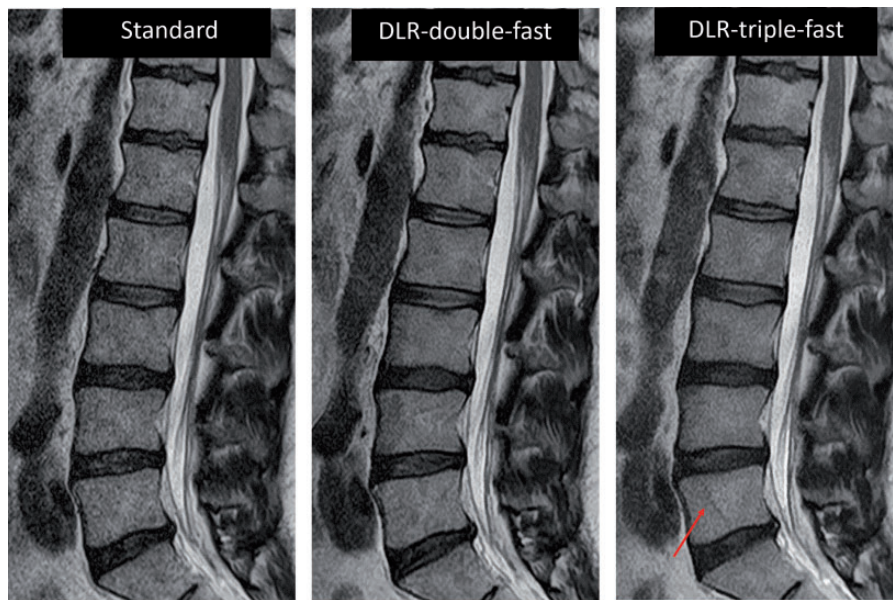
Fig. 6. Visual comparison between standard image and DLR-applied accelerated images. DLR-applied accelerated images (DLR-double-fast and DLR-triple fast) show equal or greater visual quality relative to standard image. However, a subtle streaky artifact appears in DLR-triple-fast (arrow).
DLR: deep learning-based reconstruction.

Our study has several limitations. First, we evaluated the performance of the DLR when applied only to T2-weighted MR images because it is key sequence for the diagnosis of various spinal disorders.[26] Although the preceding study using a 3T machine showed applicability of the DLR to various sequences, including T2-weighted, fluid-attenuated inversion recovery and 3D-magnetization-prepared rapid acquisition with gradient echo, we could not confirm whether the DLR maintains the expected performance in sequences with a lower SNR aimed at providing functional information, such as diffusion-weighted images or arterial spin labeling perfusion images.[15] Therefore, further studies are warranted to evaluate the DLR performance in

these sequences. Second, we did not evaluate any pathological lesions in the current study. Therefore, a study of the diagnostic accuracy of applying the DLR to MR imaging of various disorders using accelerated sequences is warranted.

In conclusion, our data suggest that application of the DLR trained by 3T brain and knee MR images applied to 1.5T lumbar MR images allow the scanning time to be shortened by one-half with adequate preservation of image quality. The combination with compressed sensing may allow the scanning time to be shortened by one-third without sacrificing image quality.

Ethics approval

Consent to participate

Authors' contributions

Acknowledgement

Declaration of Conflicting Interests

Funding

ORCID iDs
Nobuo Kashiwagi https://orcid.org/0000-0003-0986-6532
Yoshimori Kassai https://orcid.org/0000-0003-1270-8084

References
1. Gondola L. Medical image denoising using convolutional denoising autoencoders. In: *IEEE 16th International Conference on Data Mining Workshops (ICDMW)*, Barcelona, Spain, 2016, pp.241–246. IEEE.
2. Zhang K, Zuo W, Chen Y, et al. Beyond a Gaussian denoiser: residual learning of deep CNN for image denoising. IEEE Trans Image Process 2017;26:3142–3315.
3. Jiang D, Dou W, Vosters L, et al. Denoising of 3D magnetic resonance images with multi-channel residual learning of convolutional neural network. Jpn J Radiol 2018;36:566–574.
4. Wang H, Zheng R, Dai F, et al. High-field MR diffusion-weighted image denoising using a joint denoising convolutional neural network. J Magn Reson Imaging 2019;50:1937–1947.
5. Xie D, Li Y, Yang H, et al. Denoising arterial spin labeling perfusion MRI with deep machine learning. Magn Reson Imaging 2020;68:95–105.
6. Kim KH, Choi SH, Park SH. Improving arterial spin labeling by using deep learning. Radiology 2018;287:658–666.
7. Kawamura M, Tamada D, Funayama S, et al. Accelerated acquisition of high-resolution diffusion-weighted imaging of the brain with a multi-shot echo-planar sequence: deep-learning-based denoising. Magn Reson Med Sci 2021;20:99–105.
8. Han Y, Yoo J, Kim HH, et al. Deep learning with domain adaptation for accelerated projection-reconstruction MR. Magn Reson Med 2018;80:1189–1205.
9. Hammernik K, Klatzer T, Kobler E, et al. Learning a variational network for reconstruction of accelerated MRI data. Magn Reson Med 2018;79:3055–3071.
10. Eo T, Jun Y, Kim T, et al. KIKI-net: cross-domain convolutional neural networks for reconstructing undersampled magnetic resonance images. Magn Reson Med 2018;80:2188–2201.
11. Jun Y, Eo T, Shin H, et al. Parallel imaging in time-of-flight magnetic resonance angiography using deep multi-stream convolutional neural networks. Magn Reson Med 2019;81:3840–3853.
12. Hales PW, Pfeuffer J, Clark CA. Combined denoising and suppression of transient artifacts in arterial spin labeling MRI using deep learning. J Magn Reson Imaging 2020;52:1413–1426.
13. You X, Cao N, Lu H, et al. Denoising of MR images with Rician noise using a wider neural network and noise range division. Magn Reson Imaging 2019;64:154–159.
14. Lin DJ, Johnson PM, Knoll F, et al. Artificial intelligence for MR image reconstruction: an overview for clinicians. J Magn Reson Imaging 2021;53:1015–1028.
15. Kidoh M, Shinoda K, Kitajima M, et al. Deep learning-based noise reduction for brain MR imaging: tests on phantoms and healthy volunteers. Magn Reson Med Sci 2019;19:195–206.
16. Uetani H, Nakaura T, Kitajima M, et al. A preliminary study of deep learning-based reconstruction specialized for denoising in high-frequency domain: usefulness in high-resolution three-dimensional magnetic resonance cisternography of the cerebellopontine angle. Neuroradiology 2021;63:63–71.
17. Ueda T, Ohno Y, Yamamoto K, et al. Compressed sensing and deep learning reconstruction for women's pelvic MRI denoising: utility for improving image quality and examination time in routine clinical practice. Eur J Radiol 2021;134:109430.

18. Vranic JE, Cross NM, Wang Y, et al. Compressed Sensing-Sensitivity Encoding (CS-SENSE) accelerated brain imaging: reduced scan time without reduced image quality. AJNR Am J Neuroradiol 2019;40:92–98.

19. Benjamini Y and Hochberg Y. Controlling the false discovery rate: a practical and powerful approach to multiple testing. J Royal Statist Soc 1995;57:289–300.

20. Takahashi M, Uematsu H, Hatabu H. MR imaging at high magnetic fields. Eur J Radiol 2003;46:45–52.

21. Maubon AJ, Ferru JM, Berger V, et al. Effect of field strength on MR images: comparison of the same subject at 0.5, 1.0, and 1.5 T. Radiographics 1999;19: 1057–1067.

22. Dietrich O, Raya JG, Reeder SB, et al. Measurement of signal-to-noise ratios in MR images: influence of multichannel coils, parallel imaging, and reconstruction filters. J Magn Reson Imaging 2007;26:375–385.

23. Axel L. Surface coil magnetic resonance imaging. J Comput Assist Tomogr 1984;8:381–384.

24. Ding Y, Ying L, Zhang N, et al. Noise behavior of MR brain reconstructions using compressed sensing. *Annu Int Conf IEEE Eng Med Biol Soc* 2013;2013:5155–5158.

25. Jaspan ON, Fleysher R, Lipton ML. Compressed sensing MRI: a review of the clinical literature. Br J Radiol 2015;88:20150487.

26. Keerthivasan MB, Winegar B, Becker JL, et al. Clinical utility of a novel ultrafast T2-weighted sequence for spine imaging. AJNR Am J Neuroradiol 2018;39:1568–1575.